Circular Dichroism in Rotating Particles

Deng Pan,[1,*] Hongxing Xu,[2] and F. Javier García de Abajo[1,3,†]
[1]ICFO-Institut de Ciencies Fotoniques, The Barcelona Institute of Science and Technology, 08860 Castelldefels (Barcelona), Spain
[2]School of Physics and Technology, Wuhan University, Wuhan 430072, China
[3]ICREA-Institució Catalana de Recerca i Estudis Avançats, Passeig Lluís Companys 23, 08010 Barcelona, Spain

(Received 3 March 2019; published 9 August 2019)

Light interaction with rotating nanostructures gives rise to phenemona as varied as optical torques and quantum friction. Surprisingly, the most basic optical response function of nanostructures undergoing rotation has not been clearly addressed so far. Here we reveal that mechanical rotation results in circular dichroism in optically isotropic particles, which show an unexpectedly strong dependence on the particle internal geometry. More precisely, particles with one-dimensionally confined electron motion in the plane perpendicular to the rotation axis, such as nanorings and nanocrosses, exhibit a splitting of 2Ω in the particle optical resonances, while compact particles, such as nanodisks and nanospheres, display weak circular dichroism. We base our findings on a quantum-mechanical description of the polarizability of rotating particles, incorporating the mechanical rotation by populating the particle electronic states according to the principle that they are thermally equilibrated in the rotating frame. We further provide insight into the rotational superradience effect and the ensuing optical gain, originating in population inversion as regarded from the lab frame, in which the particle is out of equilibrium. Surprisingly, we find the optical frequency cutoff for superradiance to deviate from the rotation frequency Ω. Our results unveil a rich, unexplored phenomenology of light interaction with rotating objects, which might find applications in various fields, such as optical trapping and sensing.

DOI: 10.1103/PhysRevLett.123.066803

Intriguing chirality-dependent phenomena emerge during the interaction between circularly polarized light and rotating objects. For example, the rotational Doppler effect [1–6] causes emission of right- and left-circularly polarized (RCP and LCP) light from a particle rotating at frequency Ω to experience opposite frequency shifts $\pm\Omega$ [1,2]. As a consequence, inelastic scattering from anisotropic rotating particles present chiral asymmetry consisting of $\pm 2\Omega$ frequency shifts for RCP/LCP light [1,5], as observed through rotational Raman scattering [1,6]. Chiral effects are also found in elastic scattering by isotropic rotating media, such as the rotational photon drag (i.e., the rotation of polarization upon light transmission [7], which can be enhanced in slow-light media [8]). In the extreme situation when the rotation frequency exceeds the optical frequency of an incident circularly polarized light, losses in the medium turn into gains, essentially producing light amplification (the so-called superradience) at the expense of mechanical energy [9–12]. Additionally, rotation-induced chirality produces a friction torque upon interaction with the fluctuating vacuum electromagnetic field [13–19].

These phenomena are important in fundamental physics and for potential applications, such as the rotational Doppler effect, which offers a direct way to measure the rotation frequency [6]. For small objects compared with the wavelength, the rotation-dependent polarizability $\alpha(\omega)$ is the fundamental quantity in terms of which one can describe rotation-induced optical phenomena, but surprisingly, it has not been rigorously determined so far in such systems. One might naively use values of $\alpha(\omega)$ obtained from the particle at rest and apply them to the rotating particle by a simple coordinate transformation, ignoring changes in the internal states that are produced by rotation. However, such a widely used prescription [13,15,16,18,20–24] does not produce the correct frequency shifts, as we demonstrate in this paper. A more rigorous approach to model $\alpha(\omega)$ quantum mechanically then becomes necessary. To this end, a new theoretical method is needed, which is capable of describing the interaction between light and the mechanical rotation of an object, going beyond previous studies, which only treat the rotational quantum systems as isolated from the external light field [25–30].

In this Letter, we study the optical response of optically isotropic rotating particles. In particular, we obtain polarizabilities for particles of two characteristic shapes (disks and rings) rotating around their symmetry axis by applying quantum theory. The calculated results for these two types of particles reveal a general difference in the optical response between particles confined in one-dimension and compact geometries. Although both types of particles share an optical isotropy in the plane perpendicular to the rotation axis, their optical responses toward circularly polarized light shows strikingly different behaviors, characterized by a resonance shift of $\pm\Omega$ in rings and no

splitting in disks at small rotation frequency Ω. In classical terms, we attribute this discrepancy to the blocking of the Coriolis force in thin rings due to the constrained 1D motion of internal electrons, in contrast to 2D electron motion in the disks. From a quantum-mechanical perspective, the effect is equivalently explained from the change in electronic state energies in the frame rotating with the particle, where thermal equilibrium is internally established. Further intriguing conclusions are established based on our model of the optical frequency cutoff for superradiance, which we find to significantly deviate from Ω. These results open unexpected perspectives on the optical response of rotating objects.

Dichroism of rotating particles.—We consider particles that are optically isotropic for polarization perpendicular to z (Fig. 1). Two degenerate dipolar modes can then be individually excited with polarization $\mathbf{p}_{\pm}(\omega) = (\hat{x} \pm i\hat{y})p_{\pm}(\omega)/\sqrt{2}$ in the perpendicular plane in response to the electric field $\mathbf{E}_{\pm}(\omega) = (\hat{x} \pm i\hat{y})E_{\pm}(\omega)/\sqrt{2}$ of RCP (+) and LCP (−) light incident along z [bottom arrows in Fig. 1(a)]. We consider a weak field, which allows us to write $p_{\pm}(\omega) = \alpha_{\pm}(\omega)E_{\pm}(\omega)$, where $\alpha_{\pm}(\omega)$ are the corresponding linear circular polarizability components of the particle. In the absence of rotation ($\Omega = 0$), the particle is chirally symmetric, $\alpha^0_+(\omega) = \alpha^0_-(\omega) = \alpha^0(\omega)$,

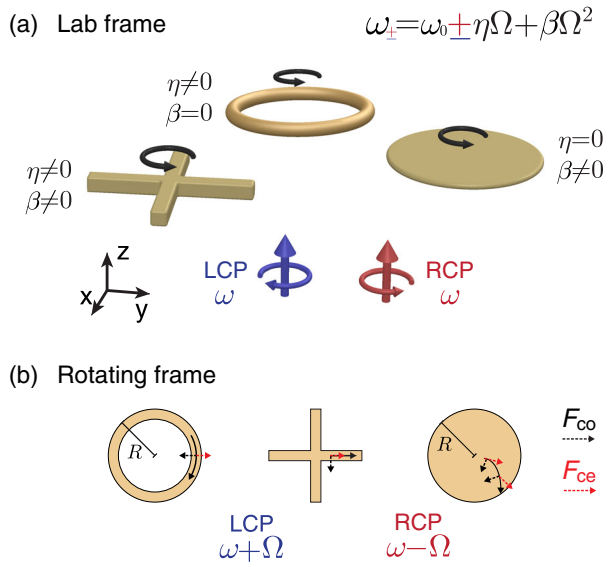

FIG. 1. We consider optically isotropic particles characterized by a resonance frequency ω_0 when they are at rest. (a) When the particles rotate with angular velocity Ω, the optical resonance frequency becomes $\omega_{\pm} = \omega_0 \pm \eta\Omega + \beta\Omega^2$ for RCP (+) and LCP (−) illumination in the lab frame (both equal to ω_0 at $\Omega = 0$), where the shape-dependent η and β terms are corrections due to Coriolis and centrifugal forces, respectively. (b) In the frame rotating with the particles, internal electrons experience Coriolis (F_{co}) and centrifugal (F_{ce}) forces, while the apparent frequency of circularly polarized incident light shifts to $\omega \mp \Omega$. The effect of F_{co} and F_{ce} depends on particle morphology.

and characterized by a spectrally isolated resonance ω_0 showing up as a degenerate peak in $\mathrm{Im}\{\alpha^0_{\pm}(\omega)\}$.

When the particle rotates at a frequency Ω around the z axis, the resonance frequencies of the two dipolar modes $p_{\pm}(\omega)$ are shifted to $\omega_{\pm} = \omega_0 \pm \eta\Omega + \beta\Omega^2$, where η and β depend on particle geometry (see below), and the sign in front of η denotes an optical circular dichroism (CD). To intuitively understand these shifts, we view the system within the frame rotating with the particle [Fig. 1(b)], in which particle electrons experience Coriolis and centrifugal forces, F_{co} and F_{ce}, respectively. The Coriolis force is a classical manifestation of Berry's phase, closely related to the magnetization of materials by rotation [31–33] and topological nontrivial phenomena [34,35]. The direction of F_{co} depends on the sign of Ω, giving rise to a correction $\pm\eta\Omega$, where η determines the magnitude of the resulting CD. In contrast, the centrifugal force always points toward the outward radial direction, and therefore, its contribution (a quadratic correction $\beta\Omega^2$) is independent of the sign of Ω. In a thin nanoring, internal electrons are confined to the ring circumference, so their motion is not affected by the forces F_{co} and F_{ce} [Fig. 1(b)]; consequently, the nanoring polarizability observed in the rotating frame must coincide with the polarizability of the motionless ring $\alpha^0(\omega)$, characterized by a ω_0 resonance. However, the coordinate transformation associated with rotation makes the frequency ω of RCP and LCP light in the lab to appear as $\omega \mp \Omega$ in the rotating frame [bottom labels in Figs. 1(a) and 1(b)], thus Doppler shifting the resonance captured by $p_{\pm}(\omega)$ to $\omega_{\pm} = \omega_0 \pm \Omega$ in the lab frame. Similar considerations also lead to a 2Ω resonance splitting in the lab frame for a rotating thin nanocross, where geometrical confinement disables F_{co}, while F_{ce} produces identical shifts in both frequencies $\omega_{\pm}$. In contrast, in extended particles such as disks [Fig. 1(b)], both F_{co} and F_{ce} affect electron motion, leading to a more complex dependence of $\alpha(\omega)$ on rotation (see below); in particular, in a free-electron description of a disk, the Coriolis force completely compensates the rotational Doppler effect, rendering $\eta = 0$ (i.e., no CD). In a disk rotating at high frequency, the centrifugal force F_{ce} pushes the electron density toward the edge, thus leading to a ringlike configuration that enhances CD.

Quantum description of rotating particles.—We model the polarizabilities $\alpha_{\pm}(\omega)$ of nanorings and nanodisks in the random-phase approximation (RPA) [36] (see details in the Supplemental Material [37]), which makes calculations feasible for systems containing many electrons and is widely used to explain experimental observations [41,42]. Because of axial symmetry, each internal one-electron state of the particle $|j\rangle$ (wave function ψ_j) has a well-defined azimuthal quantum number m_j. Provided the particle size is much smaller than the wavelength, we neglect retardation in the internal description of the particle, and accordingly represent the external circularly polarized light through a

scalar potential $\phi_{\pm}^{\rm ext}(\mathbf{r}) = -E^{\rm ext}Re^{\pm i\varphi}/\sqrt{2}$, where we use cylindrical coordinates $\mathbf{r} = (R, \varphi, z)$ and implicitly assume a time dependence $e^{-i\omega t}$. The charge distribution induced in the particle $\rho_{\pm}(\mathbf{r}) = \int d\mathbf{r}'\chi(\mathbf{r},\mathbf{r}')\phi_{\pm}^{\rm ext}(\mathbf{r}')$ is related to the potential through the susceptibility $\chi(\mathbf{r},\mathbf{r}')$, while the sought-after polarizabilities reduce to $\alpha_{\pm}(\omega) = \int d\mathbf{r}Re^{\mp i\varphi}\rho(\mathbf{r})/E^{\rm ext}$. Using matrix notation, we write $\chi = \chi^0\cdot(1 - v\cdot\chi^0)^{-1}$ in terms of the Coulomb interaction $v(\mathbf{r},\mathbf{r}') = 1/|\mathbf{r}-\mathbf{r}'|$ and the noninteracting susceptibility $\chi^0(\mathbf{r},\mathbf{r}')$. In the RPA, the latter admits the expression [36]

$$\chi^0(\mathbf{r},\mathbf{r}') = \frac{2e^2}{\hbar}\sum_{jj'}(f_{j'} - f_j)\frac{\psi_j(\mathbf{r})\psi_j^*(\mathbf{r}')\psi_{j'}^*(\mathbf{r})\psi_{j'}(\mathbf{r}')}{\omega - (E_j - E_{j'})/\hbar + i\gamma}, \quad (1)$$

where E_j and f_j denote the energy and population of state $|j\rangle$, γ is a phenomenological damping rate, and the factor of 2 accounts for spin degeneracy.

The particle rotation frequency Ω enters Eq. (1) through the populations f_j. Incidentally, a recent proposal for a quantum time crystal based on the emergence of an observable that is rotating in the lab frame [25–28] has been proven to be realizable only if the system is out of thermal equilibrium. But here we assume thermal equilibrium, which must be fulfilled in the rotating frame. In order to determine f_j, we thus need to transform the Schrödinger equation from the lab frame [coordinates (R,φ,z,t)] to the rotating frame [coordinates $(R',\varphi',z',t') = (R,\varphi-\Omega t,z,t)$], where it becomes $(\mathcal{H}_0 - \Omega\mathcal{L}_z)\psi = i\hbar\partial_t\psi$. Here, $\mathcal{H}_0$ is the Hamiltonian of the motionless particle, while the term $-\Omega\mathcal{L}_z$ accounts for $F_{\rm co}$ and $F_{\rm ce}$. For axially symmetric particles, the energies of electron states $|j\rangle$ are shifted from E_j in the motionless particle to $\tilde{E}_j = E_j - m_j\hbar\Omega$ in the rotating frame, and their populations described by the Fermi-Dirac distribution $f_j = [e^{(\tilde{E}_j - \tilde{E}_F)/k_BT} + 1]^{-1}$, where $\tilde{E}_F$ is the Fermi energy in the rotating frame. We note that Eq. (1) is general and can be used to study rotating particles of arbitrary geometry. In this study, we focus on axially symmetric particles to obtain a rigorous, analytical proof of the mechanisms discussed in Fig. 1.

Polarizability of rotating nanorings.—The population f_j in a thin rotating nanoring is illustrated in Fig. 2(a), and the resulting polarizabilities are plotted in Fig. 2(b). Neglecting radial degrees of freedom, we label electron states by the azimuthal quantum numbers m, and write the associated energies in the lab frame as $E_m = \hbar^2m^2/2m_ea^2$ [Fig. 2(a), solid curve]. For rotation at frequency Ω, the populations f_m [Fig. 2(a), red shaded area] are determined by the energies $\tilde{E}_m = E_m - m\hbar\Omega$ observed in the rotating frame [Fig. 2(a), dashed curve], so the maximum population appears at the ground state $|m_0\rangle$ in that frame. The particle rotation is evident by the nonzero total angular momentum $2\sum_m f_m m\hbar$ in this distribution. It is interesting to note that a population inversion exists in the lab frame for

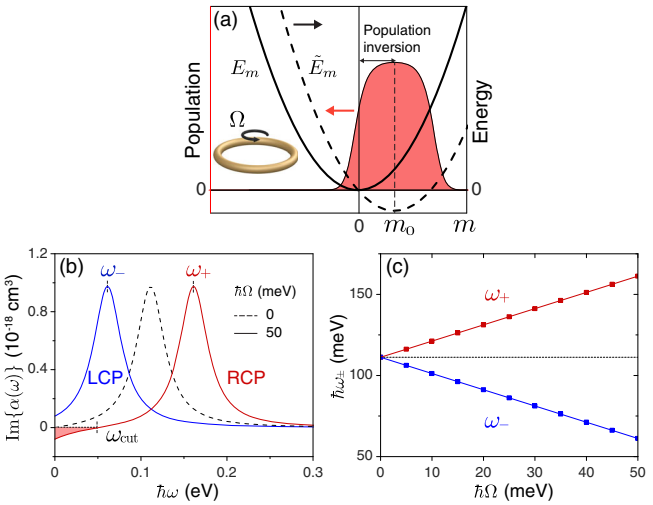

FIG. 2. (a) Energy spectra (black curves) and thermal population (red shaded curve) of the electron states $|m\rangle$ in a quasi-one-dimensional nanoring. Solid and dashed black curves correspond to electron states in the ring observed in the lab frame (energies E_m) and in a frame rotating at a frequency Ω (energies $\tilde{E}_m$), respectively. If the ring rotates at frequency Ω, its internal states are in thermal equilibrium in the rotating frame, so the population f_m of states $|m\rangle$ is determined by $\tilde{E}_m$. (b) Quantum-mechanical results for the LCP and RCP polarizability tensor components of a rotating nanoring (radius $a = 8$ nm, 80 electrons, damping $\hbar\gamma = 20$ meV) for $\hbar\Omega = 50$ meV. Results for the motionless particle (dashed curve) are displayed for comparison. The particle temperature is taken to be 300 K. (c) Position of the resonance frequencies for LCP and RCP light as a function of rotation frequency.

electron states in the $0 < m < m_0$ region. Stimulated emission from these states occurs under external illumination with suitable polarization, therefore leading to amplification of the light intensity.

Figure 2(b) shows the polarizabilites $\alpha_{\pm}(\omega)$ of a rotating nanoring (radius $a = 8$ nm, 80 electrons confined in its circumference), calculated in the RPA model discussed above. Their spectral profiles are just translations of the motionless polarizability $\alpha^0(\omega)$ [Fig. 2(b), black-dashed curve], $\alpha_{\pm}(\omega) = \alpha^0(\omega \mp \Omega)$. For $\Omega > 0$ and RCP light (or equivalently for $\Omega < 0$ and LCP light), we have $\mathrm{Im}\{\alpha_+(\omega)\} < 0$ [Fig. 2(b), red area] at frequencies ω below a cutoff $\omega_{\rm cut} = \Omega$. As the extinction cross section is proportional to the imaginary part of the polarizability, a negative value of the latter indicates that the particle produces optical gain for the incident RCP light of frequency $\omega < \Omega$; this gain originates in the population inversion observed in Fig. 2(a). Incidentally, the magnitude of $|\mathrm{Im}\{\alpha_+(\omega)\}|$ at low frequency scales with the damping rate γ [see Eq. (1)] because this parameter determines how fast out-of-equilibrium electrons [Fig. 2(a)] can undergo transitions accompanied by the emission of radiation. The rotating nanoring also shows an optical CD, the magnitude of which scales linearly with Ω in

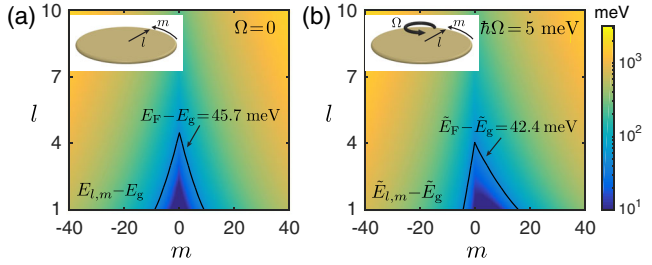

FIG. 3. (a) Energy spectrum of a nanodisk (radius $a = 12$ nm) observed in the lab frame, where m and l denote azimuthal and radial quantum numbers. The black curve shows the Fermi level when the disk contains 80 electrons. (b) Energy spectrum in a rotating frame for the disk in (a) with $\hbar\Omega = 5$ meV. The ground state shifts from $|l, m\rangle = |1, 0\rangle$ in the lab frame to $|1, 4\rangle$ in the rotating frame. Energies are referred to the respective ground state energies E_g and $\tilde{E}_g$.

accordance with the intuitive picture in Fig. 1, as illustrated in Fig. 2(c), where we plot the resonance frequencies $\omega_\pm = \omega_0 \pm \Omega$ for RCP and LCP light, so in fact a rotation frequency much smaller than the value of 50 meV used in Fig. 2(b) should be enough to manifest CD. We also note that a clear CD splitting in the spectral profiles of magnitude $2\Omega > \gamma$ should be feasible because Ω characterizes the collective motion of electrons, which is independent of the internal collision rate γ.

Polarizability of rotating nanodisks.—For a nanodisk (Fig. 3), in addition to the azimuthal quantum number m, the electron states are also labeled by a radial quantum number l, so that their energies in the motionless particle are $E_{lm} = \hbar^2\xi_{lm}^2/2a^2m_e$, where ξ_{lm} is the lth zero of the Bessel function J_m. We assume a single out-of-plane electron state for simplicity. The energies E_{lm} are represented in Fig. 3(a) for a disk of radius $a = 12$ nm; the ground state is then $|l, m\rangle = |1, 0\rangle$ ($E_g = 1.5$ meV) and the Fermi energy (black curve) is $E_F = 47.2$ meV when the disk is filled with 80 electrons, which is experimentally attainable by etching a lightly doped thin semiconductor layer. The electron energies in a nanodisk observed in a frame rotating with frequency Ω become $\tilde{E}_{lm} = E_{lm} - m\hbar\Omega$. These energies are represented in Fig. 3(b) for the same disk as in (a) and $\hbar\Omega = 5$ meV; the ground state energy ($\tilde{E}_g = -4.8$ meV) has now moved to $|1, 4\rangle$ and the Fermi energy becomes $\tilde{E}_F = 37.6$ meV. If this disk is also rotating at frequency Ω, the internal state populations f_{lm} follow a Fermi-Dirac distribution determined by the rotating frame energies $\tilde{E}_{lm}$ shown in Fig. 3(b).

Figure 4(a) shows the polarizability $\mathrm{Im}\{\alpha(\omega)\}$ computed from Eq. (1) for different rotation velocities. Surprisingly, the cutoff frequency ω_{cut} for superradience [Fig. 4(b)] presents substantial deviations from Ω, including its slope as a function of Ω at small rotation frequencies. Additionally, the resulting CD differs considerably in the rotating nanodisk compared with the rotating nanoring, as found upon inspection of the resonance frequencies $\omega_\pm$ [Fig. 4(c)] and the magnitude at the peaks of $\mathrm{Im}\{\alpha(\omega)\}$ [Fig. 4(d)]. At relatively low rotation frequencies ($|\hbar\Omega| < 10$ meV), $\omega_\pm$ deviate slightly from ω_0, so the resulting CD has a small magnitude. We explain this effect by considering the Coriolis force F_{co} in the rotating frame, which produces an effective magnetization on the particle, resulting in frequency shifts $\mp\Omega$ that compensate the rotational Doppler shifts $\pm\Omega$. We further attribute small deviations from perfect compensation to the asymmetry of the Fermi energy in the rotating particle [i.e., the change in populations f_{lm} observed in Fig. 3(b)].

The conservative centrifugal force defines an effective potential that pushes the electron density toward the disk edge (for tutorial purposes, we disregard the self-consistent Hartree interaction among electrons in the disk, although this interaction can reduce edge charge accumulation, as shown in the Supplemental Material [37]). This effect (β term in Fig. 1) produces an identical frequency shift in $\omega_\pm$; it additionally leads to a ringlike configuration (electrons confined near the edges), which becomes significant at high Ω (notice the Ω^2 scaling of F_{ce}), and its interplay with the Coriolis force results in a CD even stronger than in the ring ($|\omega_+ - \omega_-| > 2\Omega$). Furthermore, all features of the rotation-dependent polarizabilities are corroborated by an extension of the Drude model incorporating Coriolis (see the Supplemental Material for details [37]). This semiclassical model can be easily applied to particles of

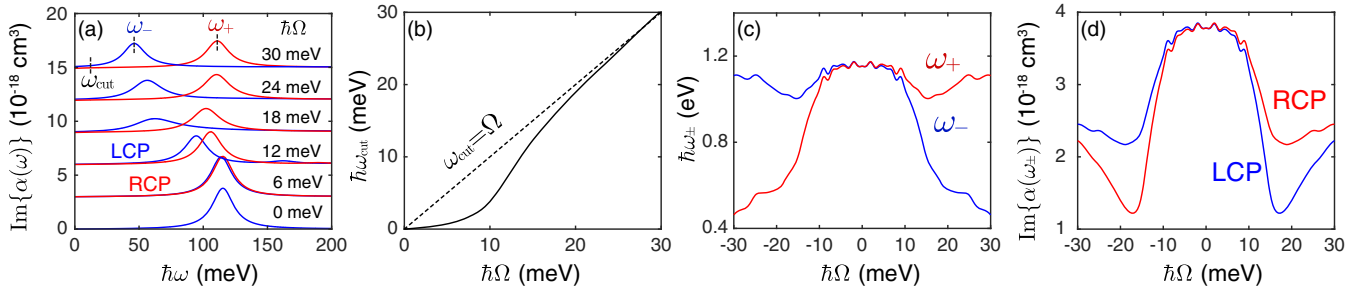

FIG. 4. (a) Polarizability of a disk (radius $a = 12$ nm, 80 electrons, damping $\hbar\gamma = 10$ meV) rotating at different frequencies Ω (see labels) for LCP (blue) and RCP (red) light. (b) Rotation-frequency dependence of the cutoff for superradiance. (c),(d) Ω dependence of the resonance frequency $\omega_\pm$ (c) and maximum polarizability (d) extracted from (a).

arbitrary geometry, as shown for a rotating nanocross in the Supplemental Material [37], further confirming the mechanisms discussed in Fig. 1.

Concluding remarks.—We investigate the polarizability of optically isotropic rotating particles, which reveals a strong dependence of their response on the particle geometry. Our formalism traces this finding back to the out-of-equilibrium distribution of the particle electronic state as observed in the lab frame, which affects the way in which they exchange energy and momentum with the surrounding vacuum. The frame-dependent thermal equilibration here revealed relates the classical motion of a microscopic object to the internal thermal population of its relevant constituents (electrons in this study). Our model successfully describes the interaction between a rotating quantum system and an external light field, which is instructive for future efforts attempting to explain optomechanical processes based on first principles. Considering that small particles have been observed to rotate at gigahertz frequencies [43,44], their exotic shape-dependent CD under rotation leads to measurable splittings on their resonances using currently available techniques. Narrow excitation lines such as those associated with dopant two-level emitters could be used for this purpose. Alternatively, doped graphene structures should facilitate the task because of their high electrical tunability and the long lifetime of their plasmons [45] (see Supplemental Material e.g., [37]). Additionally, a graphene disk of ∼100 nm radius should mechanically resist high rotation frequencies [46]. Since the predicted effect lies in the out-of-equilibrium particle distribution in the lab frame, an effective rotation could be also achieved through an electric current circulating around a graphene ring; instantaneous rotation could be mimicked by pumping particle electrons to a nonequilibrium state with nonzero angular momentum through an ultrafast circularly polarized pulse, and the resulting CD should be measurable in a pump-probe experiment.

Predictions in this study may lead to new approaches in various application fields. For example, a linearly polarized laser can exert a torque on a rotating particle due to the rotational CD (similar to the torque exerted by linearly polarized light acting on motionless chiral particles [47]), which offers new mechanisms for influencing the particle motion, and could thus be eventually developed to produce optical trapping; the rotational CD effect constitutes a mechanism to measure the rotating frequency of axially symmetric particles, in which the rotational Doppler effect is absent; geometry-dependent rotational CD further provides a method to reveal the internal morphology of the rotating particles; the effective rotation mimicked by an electric current circulating around a graphene ring could be used as a compact platform for electrically controlling the polarization of infrared light, and an array of these units could realize an active metasurface for image encoding.

*Corresponding author.
deng.pan@icfo.eu
†Corresponding author.
javier.garciadeabajo@nanophotonics.es

[1] B. A. Garetz, J. Opt. Soc. Am. Lett. **71**, 609 (1981).
[2] J. Courtial, K. Dholakia, D. A. Robertson, L. Allen, and M. J. Padgett, Phys. Rev. Lett. **80**, 3217 (1998).
[3] J. Courtial, D. A. Robertson, K. Dholakia, L. Allen, and M. J. Padgett, Phys. Rev. Lett. **81**, 4828 (1998).
[4] V. C. Chen, F. Li, S.-S. Ho, and H. Wechsler, IEEE Trans. Aerosp. Electron. Syst. **42**, 2 (2006).
[5] M. P. Lavery, F. C. Speirits, S. M. Barnett, and M. J. Padgett, Science **341**, 537 (2013).
[6] O. Korech, U. Steinitz, R. J. Gordon, I. S. Averbukh, and Y. Prior, Nat. Photonics **7**, 711 (2013).
[7] M. Padgett, G. Whyte, J. Girkin, A. Wright, L. Allen, P. Öhberg, and S. M. Barnett, Opt. Lett. **31**, 2205 (2006).
[8] S. Franke-Arnold, G. Gibson, R. W. Boyd, and M. J. Padgett, Science **333**, 65 (2011).
[9] V. Ginzburg and I. Frank, Dokl. Akad. Nauk SSSR **56**, 583 (1947).
[10] Y. B. Zel'Dovich, Sov. Phys. JETP **35**, 1085 (1972).
[11] J. D. Bekenstein and M. Schiffer, Phys. Rev. D **58**, 064014 (1998).
[12] A. Asenjo-Garcia, A. Manjavacas, and F. J. García de Abajo, Phys. Rev. Lett. **106**, 213601 (2011).
[13] A. Manjavacas and F. J. García de Abajo, Phys. Rev. Lett. **105**, 113601 (2010).
[14] R. A. Álvarez-Puebla, L. M. Liz-Marzán, and F. J. García de Abajo, J. Phys. Chem. Lett. **1**, 2428 (2010).
[15] R. Zhao, A. Manjavacas, F. J. García de Abajo, and J. B. Pendry, Phys. Rev. Lett. **109**, 123604 (2012).
[16] M. F. Maghrebi, R. L. Jaffe, and M. Kardar, Phys. Rev. Lett. **108**, 230403 (2012).
[17] H. Bercegol and R. Lehoucq, Phys. Rev. Lett. **115**, 090402 (2015).
[18] A. Manjavacas, F. J. Rodríguez-Fortuño, F. J. García de Abajo, and A. V. Zayats, Phys. Rev. Lett. **118**, 133605 (2017).
[19] D. Pan, H. Xu, and F. J. García de Abajo, Phys. Rev. A **99**, 062509 (2019).
[20] A. Manjavacas and F. J. García de Abajo, Phys. Rev. A **82**, 063827 (2010).
[21] M. F. Maghrebi, R. Golestanian, and M. Kardar, Phys. Rev. A **88**, 042509 (2013).
[22] M. F. Maghrebi, R. Golestanian, and M. Kardar, Phys. Rev. D **87**, 025016 (2013).
[23] M. F. Maghrebi, R. L. Jaffe, and M. Kardar, Phys. Rev. A **90**, 012515 (2014).
[24] S. Lannebère and M. G. Mário, Phys. Rev. A **94**, 033810 (2016).
[25] F. Wilczek, Phys. Rev. Lett. **109**, 160401 (2012).
[26] T. Li, Z.-X. Gong, Z.-Q. Yin, H. T. Quan, X. Yin, P. Zhang, L.-M. Duan, and X. Zhang, Phys. Rev. Lett. **109**, 163001 (2012).
[27] P. Bruno, Phys. Rev. Lett. **111**, 070402 (2013).
[28] H. Watanabe and M. Oshikawa, Phys. Rev. Lett. **114**, 251603 (2015).
[29] B. A. Stickler, B. Schrinski, and K. Hornberger, Phys. Rev. Lett. **121**, 040401 (2018).

[30] B. A. Stickler, F. T. Ghahramani, and K. Hornberger, Phys. Rev. Lett. **121**, 243402 (2018).
[31] S. J. Barnett, Phys. Rev. **6**, 239 (1915).
[32] S. J. Barnett, Rev. Mod. Phys. **7**, 129 (1935).
[33] S. Heims and E. Jaynes, Rev. Mod. Phys. **34**, 143 (1962).
[34] S. Weigert, Phys. Rev. Lett. **75**, 1435 (1995).
[35] Y.-T. Wang, P.-G. Luan, and S. Zhang, New J. Phys. **17**, 073031 (2015).
[36] L. Hedin and S. Lundqvist, in *Solid State Physics*, edited by D. T. Frederick Seitz and H. Ehrenreich (Academic Press, New York, 1970), Vol. 23, pp. 1–181.
[37] See Supplemental Material at http://link.aps.org/supplemental/10.1103/PhysRevLett.123.066803, where we provide additional details on the RPA formalism and calculations for disks and rings in the interacting and noninteracting pictures, as well as a self-contained derivation of the Drude model in the local limit with inclusion of Coriolis together with its application to simulate rotating graphene rings, disks, and crosses, which includes Refs. [38–40].
[38] D. Pines and P. Nozières, *The Theory of Quantum Liquids* (W.A. Benjamin, Inc., New York, 1966).
[39] A. Manjavacas and F. J. García de Abajo, Nat. Commun. **5**, 3548 (2014).
[40] A. H. Castro Neto, F. Guinea, N. M. R. Peres, K. S. Novoselov, and A. K. Geim, Rev. Mod. Phys. **81**, 109 (2009).
[41] G. Onida, L. Reining, and A. Rubio, Rev. Mod. Phys. **74**, 601 (2002).
[42] S. Thongrattanasiri, A. Manjavacas, and F. J. García de Abajo, ACS Nano **6**, 1766 (2012).
[43] R. Reimann, M. Doderer, E. Hebestreit, R. Diehl, M. Frimmer, D. Windey, F. Tebbenjohanns, and L. Novotny, Phys. Rev. Lett. **121**, 033602 (2018).
[44] J. Ahn, Z. Xu, J. Bang, Y.-H. Deng, T. M. Hoang, Q. Han, R.-M. Ma, and T. Li, Phys. Rev. Lett. **121**, 033603 (2018).
[45] G. X. Ni, A. S. McLeod, Z. Sun, L. Wang, L. Xiong, K. W. Post, S. S. Sunku, B.-Y. Jiang, J. Hone, C. R. Dean *et al.*, Nature (London) **557**, 530 (2018).
[46] C. Lee, X. Wei, J. W. Kysar, and J. Hone, Science **321**, 385 (2008).
[47] Y. Yang, P. D. Brimicombe, N. W. Roberts, M. R. Dickinson, M. Osipov, and H. F. Gleeson, Opt. Express **16**, 6877 (2008).